# Electron-Nuclear Coupling through Autoionizing States after Strong-Field Excitation of $H_2$ Molecules

Yonghao Mi,* Nicolas Camus, Lutz Fechner, Martin Laux, Robert Moshammer, and Thomas Pfeifer†
*Max-Planck-Institut für Kernphysik, Saupfercheckweg 1, 69117 Heidelberg, Germany*
(Received 19 December 2016; published 2 May 2017)

Channel-selective electron emission from strong-field photoionization of $H_2$ molecules is experimentally investigated by using ultrashort laser pulses and a reaction microscope. The electron momenta and energy spectra in coincidence with bound and dissociative ionization channels are compared. Surprisingly, we observed an enhancement of the photoelectron yield in the low-energy region for the bound ionization channel. By further investigation of asymmetrical electron emission using two-color laser pulses, this enhancement is understood as the population of the autoionizing states of $H_2$ molecules in which vibrational energy is transferred to electronic energy. This general mechanism provides access to the vibrational-state distribution of molecular ions produced in a strong-field interaction.

DOI: 10.1103/PhysRevLett.118.183201

Ultrashort laser fields can play a key role in controlling molecules and their reactions as they act on the same time scale as the electron dynamics in these systems [1]. For example, the development of the carrier-envelope-phase stabilized laser [2,3] has allowed the localization of electrons and asymmetric emission of ions in the photodissociation of simple molecules [4–8]. The Born-Oppenheimer approximation, in which electrons of a molecule are considered separated from the nuclei, is used in most of the above-mentioned works for modeling molecules, including the simplest $H_2$ molecule in strong laser fields. This gives rise to the two-step mechanism [4], which describes the laser-induced dissociation of $H_2$ molecules as follows: the molecule is ionized by the laser field in the first step and then dissociates as the vibrational wave packet is laser excited from the bound $1s\sigma_g$ state to the repulsive $2p\sigma_u$ state in most cases. To investigate the wave packet dynamics for different ionization channels, numerous studies concentrated on measurements of the ions produced after strong-field ionization of molecules (see, e.g., [9] for a review). However, this information is often not sufficient to determine the reaction pathway. One strategy for obtaining more information is to consider, in addition, the electron [10]. However, this requires the ion-electron coincidence technique which has been applied only in a limited number of strong-field experiments [11–13].

In this Letter, we report on coincident measurements of electron spectra from bound and dissociative ionization channels of $H_2$ by using a reaction microscope (REMI) [14]. We observe a clear difference between the two channels: an enhancement in photoelectron yield in the low-energy region (0–0.6 eV) that appears only in the bound ionization channel. We interpret this enhancement as a result of an electronic-internuclear coupling by a vibrational autoionization process of $H_2$ molecules. Finally, to provide additional evidence, we measure and analyze the spatial asymmetry of the electron emission by using two-color laser pulses.

In the experiment, linearly polarized 25 fs laser pulses at the central wavelength of 800 nm are generated by a commercial amplified Ti:Sapphire laser. These laser pulses are focused inside the REMI, where they intersect a supersonic skimmed $H_2$ gas jet. The initial momentum vectors of ions and electrons from different ionization channels can be reconstructed by measuring the particle flight times and their positions of detection. Measuring electrons and ions in coincidence, we can distinguish the bound and dissociative ionization channel and extract electron momenta for both channels. For the generation of phase-controllable two-color laser pulses, we use the same experimental setup as described in [15]. In brief, we generate the second harmonic and adjust its time delay relative to the fundamental laser pulse by means of a Mach-Zehnder interferometer.

Several ionization pathways may occur when $H_2$ molecules interact with a strong laser field. In this experiment, the main processes are the following two single ionization channels:

$$H_2 \xrightarrow{\mathrm{IR}} H_2^+ + e^-, \tag{1}$$

$$H_2 \xrightarrow{\mathrm{IR}} H^+ + H + e^-. \tag{2}$$

The first channel is molecular bound ionization without fragmentation, in which one electron is ionized by the laser field and the system ends up as a bound molecular ion $H_2^+$ and a free electron. The second channel is dissociative ionization, where the $H_2$ molecule breaks up into a proton, a hydrogen atom, and a free electron.

Figure 1 shows the 3D momentum distributions of electrons for the two channels ($p_\parallel$ is the momentum in

 

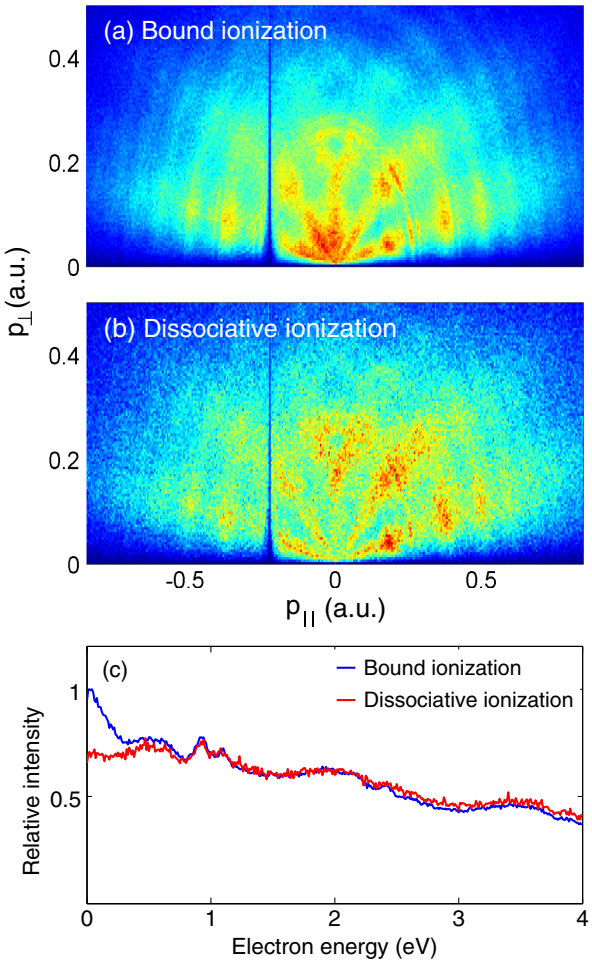


FIG. 1. Electron momentum distribution for (a) the bound ionization channel and (b) the dissociative ionization channel as measured in coincidence with $H_2^+$ and $H^+$ ions, respectively. (c) Electron-energy spectra for bound (blue curve) and dissociative (red curve) ionization.

the laser polarization direction and $p_\perp$ is the momentum in the transverse direction). The left-right asymmetry along the parallel momentum is due to nonuniform detection efficiency. The fanlike stripes and the above-threshold ionization rings in the photoelectron spectra, which are caused by intracycle and intercycle interferences [16], respectively, appear for both channels. On first approximation, if the dissociative ionization process is independent from the bound ionization process, the electrons from the two channels should be the same. However, the fanlike structure for electrons of small energy can be observed clearly in the bound ionization channel [Fig. 1(a)], while the same structure is much less pronounced in the dissociative ionization channel [Fig. 1(b)]. In order to compare electrons emitted from the two channels, we normalize the energy spectra of photoelectrons, shown in Fig. 1(c). Distinct peaks around 0.9 eV are visible for both channels. These are attributed to Freeman resonances [17–19]. The electrons from the bound ionization channel (blue curve) exhibit an enhancement in the low-energy region of the spectrum (0–0.6 eV). In the high-energy region, both normalized spectra agree within our experimental resolution. To our knowledge, this is the first observation of a clear difference in electron spectra between the bound and dissociative ionization of $H_2$ molecules in strong laser fields.

Inspired by previous experimental results in atoms [20], we interpret the low-energy enhancement in the electron yield for bound ionization as being due to the population and subsequent decay of autoionizing states. For $H_2$ molecules, the autoionizing states are singly excited states, which represent a series of high-lying Rydberg states and are characterized by a simultaneous electronic and vibrational excitation. These states with vibrational quantum number $\nu$ converge to the state of $H_2^+$ with the same vibrational quantum number $\nu$. Figure 2 shows one of the high-lying Rydberg states of $H_2^*$ (black solid line) and its first three vibrational states (black dashed lines). Details on the energy levels of these high-lying Rydberg states can be found in Refs. [21–23]. Above the ionization limit of the $H_2^+$ molecular ion ($\nu = 0$, shown by the red solid line), there exist many autoionizing states (e.g., $\nu' = 1$ and $\nu' = 2$ in Fig. 2). Instead of populating the $H_2^+$ bound state (red curve) and being excited to the repulsive state (blue curve) for dissociation, which is described by the two-step mechanism [shown as (1) and (2) in Fig. 2], the molecule is excited to the abovementioned autoionizing state located above the ionization limit [21–25]. In the autoionization process, the vibrational energy of the nuclei is transferred to the energy of the free electron and is reflected in the electron energy spectrum. As the lifetime of these

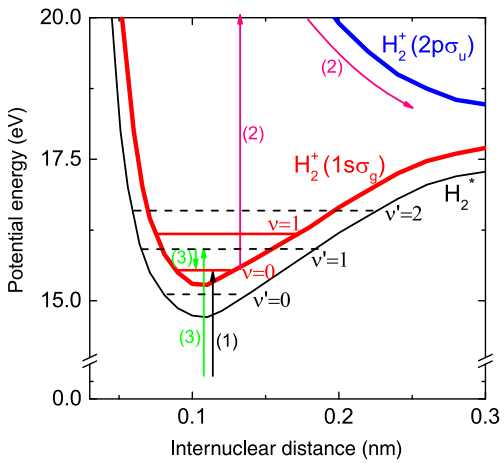


FIG. 2. Potential energy curves for one of the Rydberg states: $H_2^*$ (black curve), $H_2^+$ bound state (red curve), and $H_2^+$ repulsive state (blue curve). (1) and (2) show the main dissociation process by the two-step mechanism: the molecule is ionized by the laser field, and then, a vibrational wave packet is excited from the bound $1s\sigma_g$ state to the repulsive $2p\sigma_u$ state. (3) refers to the autoionization process in which low-energy electrons are emitted (vibrational levels are not drawn to scale).

vibrational states is more than hundreds of femtoseconds, which is much longer than the laser pulse duration, the autoionization process of $H_2$ occurs long after the strong-field excitation by the laser pulses, which explains why the autoionization does not occur for the dissociative ionization channel. Also, the corresponding autoionizing states are still lower in energy than the dissociation limit. Therefore, the enhancement in the low-energy photoelectron yield only appears for the bound ionization, not for the dissociative ionization.

The abovementioned vibrational autoionization is a process of electronic-nuclear coupling after the laser excitation, which proves that the Born-Oppenheimer approximation is not valid. It is different from the ionization of Rydberg electrons by the field of the spectrometer in which the low or zero-energy structure could be observed [26–29]. In those cases, the structures are very sharp and in a much lower energy region.

By comparing the electron energy spectrum of bound ionization in this experiment with theoretical and previous high-resolution experimental work on Rydberg states of $H_2$ [21–23,30–32], we are able to determine the vibrational states that contribute to the autoionization process. According to the propensity rule in vibrational autoionization [22,33,34], the most dominant vibrational relaxations proceed from one vibrational state to another one that differs by one vibrational quantum number

$$\Delta\nu = \nu' - \nu = 1. \tag{3}$$

For example, the energy-level diagram in Fig. 3(a) shows the energy differences between a series of $np\sigma$ and $np\pi$ Rydberg states ($\nu' = 1$) of ortho-$H_2$ and the energy of the $H_2^+$ ground state ($\nu = 0$). Similarly, the diagram in Fig. 3(b) denotes the $\nu' = 2$ Rydberg state energies after subtracting the $\nu = 1$ energy level of $H_2^+$. For comparison, we also plotted the energy diagram in Fig. 3(c) resulting from the transitions from $\nu' = 2$ Rydberg states to the $\nu = 0$ state of $H_2^+$. The photoelectron spectra from bound (blue curve) and dissociative (red curve) ionization are plotted together with the energy-level diagrams. It can be seen that photoelectrons from the $\Delta\nu = 2$ transitions contribute much less than the $\Delta\nu = 1$ transitions for the bound ionization, which agrees well with the propensity rule.

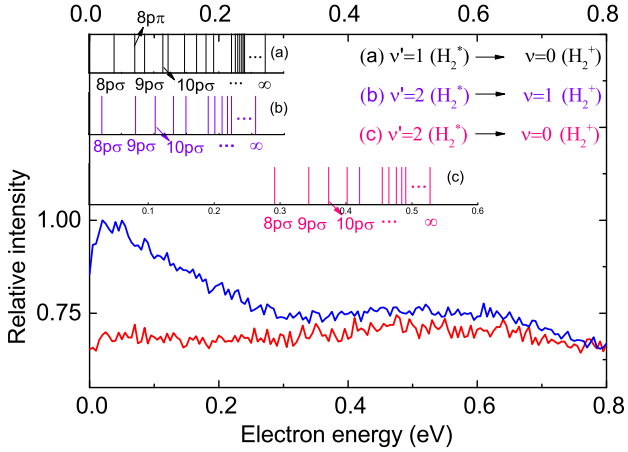


FIG. 3. Energy-level diagram of the Rydberg states ($\nu' = 1$ and $\nu' = 2$) of $H_2^*$ subtracting the first two vibrational levels ($\nu = 0$ and $\nu = 1$) of the $H_2^+$ ground state and the photoelectron energy spectra for the bound (blue curve) and dissociative (red curve) ionization.

In order to investigate in more detail the difference between bound and dissociative ionization, we performed these measurements with superpositions of two laser pulses with different colors and adjustable relative phase. Changing the relative phase between the 400 and 800 nm laser pulses allows us to shape the electric field of the pulses on attosecond time scales, making it asymmetric. For strong-field ionization, this asymmetry is typically imprinted in the electron energy and emission direction [35] or the emission direction of fragments in the dissociation process of diatomic molecules [36,37]. In the case of autoionization considered here, which happens long after the laser pulse is over, we expect the corresponding electron to be unaffected by the asymmetric field of the pulses.

To quantify the emission asymmetry, we define an asymmetry parameter $A$ as a function of the relative phase between the two-color pulses $\phi$ and the electron energy $E_e$ by the following equation:

$$A(E_e, \phi) = \frac{N_+(E_e, \phi) - N_-(E_e, \phi)}{N_+(E_e, \phi) + N_-(E_e, \phi)}, \tag{4}$$

where, $N_+(E_e, \phi)$ and $N_-(E_e, \phi)$ represent the number of electrons at the energy $E_e$ emitted, respectively, with positive and negative longitudinal momentum at the phase of $\phi$. We plot the asymmetry parameter $A$ of electrons for the bound and dissociative ionization channels, as shown in Figs. 4(a) and 4(b). The asymmetry patterns for the two channels are almost identical, as expected from the two-step mechanism. To more closely analyze these results, we fit the energy-dependent asymmetry by a sinusoidal function of the two-color phase $\phi$

$$A(\phi, E_e) = A_0(E_e)\sin[\phi + \phi_0(E_e)], \tag{5}$$

with $A_0(E_e)$ the amplitude of the asymmetry and $\phi_0(E_e)$ the offset of this asymmetry.

$A_0(E_e)$ as a function of the electron energy up to 1.5 eV is plotted for the two channels in Fig. 4(c). A large difference in the amplitude of asymmetry is observed only in the low-energy region corresponding to the autoionizing channels depicted in Fig. 3. The offset of the asymmetry $\phi_0(E_e)$ shows no difference within the error bars for the two channels. The result confirms that, for the two channels, the low-energy electrons stem from different pathways. This proves that the generally accepted two-step

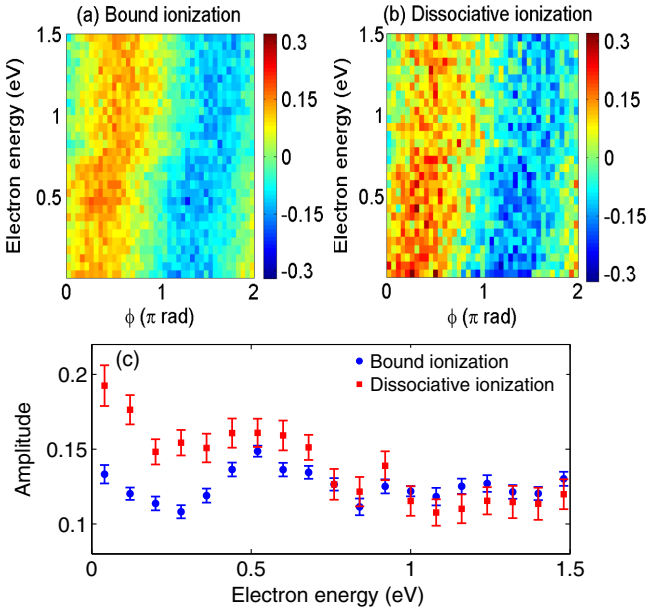


FIG. 4. Asymmetry of electrons as a function of the relative phase between the two-color fields and the electron energy for (a) bound ionization and (b) dissociative ionization. (c) The amplitude of the electron asymmetry as a function of electron energy for bound ionization (blue dot) and dissociative ionization (red square).

mechanism, which considers the dissociative ionization step separated from the first step (bound ionization), is not complete. Moreover, it supports that the origin of this low-energy region electron is from the high-lying Rydberg state.

For the bound ionization pathway, the low-energy electrons originate from two different mechanisms: (1) direct photoionization by the laser pulses and (2) vibrational autoionization after the laser pulses. However, for the dissociative ionization, the low-energy electrons only come from the direct ionization by the two-color laser pulse, and its effect on the electron momentum is mostly visible once the electron is freed within the pulse, as expected from strong-field ionization [15,38]. Since the emission of the electrons from autoionization happens long after the laser pulse is over, their directionality is not influenced by the relative phase $\phi$ between the two colors in the laser pulse and, thus, shows no asymmetry. Therefore, the amplitude of the low-energy electron asymmetry variation for the bound ionization, which is the total asymmetry amplitude of (1) and (2), has a smaller value compared to the dissociative ionization for which only the direct (asymmetry-sensitive) ionization channel exists.

In conclusion, we investigated the difference in electron emission between bound and dissociative ionization pathways by using an 800 nm laser pulse and its second harmonic. This electron-ion coincidence experiment reveals that low-energy electron emission is enhanced for bound ionization as compared to dissociative ionization. While in apparent disagreement with the widely employed Born-Oppenheimer-based two-step process, we explain this low-energy excess by the population and subsequent electron emission out of autoionizing states. Future experiments could use a pump-probe setup to directly measure the lifetimes of the contributing autoionizing states. By changing the relative phase of the two-color laser field, we find that the amplitude of asymmetry is lower for the low-energy electrons emitted in coincidence with bound molecular ions, thus, further supporting the vibrational autoionization mechanism. In the future, this mechanism can be used to explore the detailed distribution and interplay of vibrational and electronic excitation after strong-field interaction, which was not directly accessible in previous experiments.

Yonghao Mi acknowledges the support from the China Scholarship Council (CSC).

*yonghao.mi@mpi-hd.mpg.de
†thomas.pfeifer@mpi-hd.mpg.de

[1] F. Krausz and M. Ivanov, Rev. Mod. Phys. **81**, 163 (2009).
[2] G. G. Paulus, F. Grasbon, H. Walther, P. Villoresi, M. Nisoli, S. Stagira, E. Priori, and S. De Silvestri, Nature (London) **414**, 182 (2001).
[3] A. Baltuska, T. Udem, M. Uiberacker, M. Hentschel, E. Goulielmakis, C. Gohle, R. Holzwarth, V. S. Yakovlev, A. Scrinzi, T. W. Hansch, and F. Krausz, Nature (London) **421**, 611 (2003).
[4] M. F. Kling, C. Siedschlag, A. J. Verhoef, J. I. Khan, M. Schultze, T. Uphues, Y. Ni, M. Uiberacker, M. Drescher, F. Krausz, and M. J. J. Vrakking, Science **312**, 246 (2006).
[5] M. Kremer, B. Fischer, B. Feuerstein, V. L. B. de Jesus, V. Sharma, C. Hofrichter, A. Rudenko, U. Thumm, C. D. Schröter, R. Moshammer, and J. Ullrich, Phys. Rev. Lett. **103**, 213003 (2009).
[6] F. Martín, J. Fernández, T. Havermeier, L. Foucar, T. Weber, K. Kreidi, M. Schöffler, L. Schmidt, T. Jahnke, O. Jagutzki, A. Czasch, E. P. Benis, T. Osipov, A. L. Landers, A. Belkacem, M. H. Prior, H. Schmidt-Böcking, C. L. Cocke, and R. Dörner, Science **315**, 629 (2007).
[7] G. Sansone, F. Kelkensberg, J. F. Perez-Torres, F. Morales, M. F. Kling, W. Siu, O. Ghafur, P. Johnsson, M. Swoboda, E. Benedetti, F. Ferrari, F. Lepine, J. L. Sanz-Vicario, S. Zherebtsov, I. Znakovskaya, A. L'Huillier, M. Y. Ivanov, M. Nisoli, F. Martin, and M. J. J. Vrakking, Nature (London) **465**, 763 (2010).
[8] A. Fischer, A. Sperl, P. Cörlin, M. Schönwald, H. Rietz, A. Palacios, A. González-Castrillo, F. Martín, T. Pfeifer, J. Ullrich, A. Senftleben, and R. Moshammer, Phys. Rev. Lett. **110**, 213002 (2013).
[9] J. H. Posthumus, Rep. Prog. Phys. **67**, 623 (2004).
[10] V. L. B. de Jesus, B. Feuerstein, K. Zrost, D. Fischer, A. Rudenko, F. Afaneh, C. D. Schröter, R. Moshammer, and J. Ullrich, J. Phys. B **37**, L161 (2004).
[11] K. Hosaka, R. Itakura, K. Yokoyama, K. Yamanouchi, and A. Yokoyama, Chem. Phys. Lett. **475**, 19 (2009).

[12] A. E. Boguslavskiy, J. Mikosch, A. Gijsbertsen, M. Spanner, S. Patchkovskii, N. Gador, M. J. J. Vrakking, and A. Stolow, Science **335**, 1336 (2012).
[13] W. Zhang, Z. Li, P. Lu, X. Gong, Q. Song, Q. Ji, K. Lin, J. Ma, F. He, H. Zeng, and J. Wu, Phys. Rev. Lett. **117**, 103002 (2016).
[14] J. Ullrich, R. Moshammer, A. Dorn, R. Dörner, L. P. H. Schmidt, and H. Schmidt-Böcking, Rep. Prog. Phys. **66**, 1463 (2003).
[15] D. G. Arbó, C. Lemell, S. Nagele, N. Camus, L. Fechner, A. Krupp, T. Pfeifer, S. D. López, R. Moshammer, and J. Burgdörfer, Phys. Rev. A **92**, 023402 (2015).
[16] D. G. Arbó, K. L. Ishikawa, E. Persson, and J. Burgdörfer, Nucl. Instrum. Methods Phys. Res., Sect. B **279**, 24 (2012).
[17] R. R. Freeman, P. H. Bucksbaum, H. Milchberg, S. Darack, D. Schumacher, and M. E. Geusic, Phys. Rev. Lett. **59**, 1092 (1987).
[18] R. R. Freeman and P. H. Bucksbaum, J. Phys. B **24**, 325 (1991).
[19] C. M. Maharjan, A. S. Alnaser, I. Litvinyuk, P. Ranitovic, and C. L. Cocke, J. Phys. B **39**, 1955 (2006).
[20] L. Fechner, N. Camus, A. Krupp, J. Ullrich, T. Pfeifer, and R. Moshammer, Phys. Rev. A **92**, 051403 (2015).
[21] G. Herzberg and C. Jungen, J. Mol. Spectrosc. **41**, 425 (1972).
[22] M. Glass-Maujean, C. Jungen, H. Schmoranzer, I. Haar, A. Knie, P. Reiss, and A. Ehresmann, J. Chem. Phys. **135**, 144302 (2011).
[23] D. Sprecher, C. Jungen, and F. Merkt, J. Chem. Phys. **140**, 104303 (2014).
[24] V. H. Dibeler, R. M. Reese, and M. Krauss, J. Chem. Phys. **42**, 2045 (1965).
[25] C. Dimopoulou, R. Moshammer, D. Fischer, C. Höhr, A. Dorn, P. D. Fainstein, J. R. Crespo López Urrutia, C. D. Schröter, H. Kollmus, R. Mann, S. Hagmann, and J. Ullrich, Phys. Rev. Lett. **93**, 123203 (2004).
[26] J. Dura, N. Camus, A. Thai, A. Britz, M. Hemmer, M. Baudisch, A. Senftleben, C. D. Schröter, J. Ullrich, R. Moshammer, and J. Biegert, Sci. Rep. **3**, 2675 (2013).
[27] B. Wolter, C. Lemell, M. Baudisch, M. G. Pullen, X.-M. Tong, M. Hemmer, A. Senftleben, C. D. Schröter, J. Ullrich, R. Moshammer, J. Biegert, and J. Burgdörfer, Phys. Rev. A **90**, 063424 (2014).
[28] E. Diesen, U. Saalmann, M. Richter, M. Kunitski, R. Dörner, and J. M. Rost, Phys. Rev. Lett. **116**, 143006 (2016).
[29] S. Larimian, S. Erattupuzha, C. Lemell, S. Yoshida, S. Nagele, R. Maurer, A. Baltuška, J. Burgdörfer, M. Kitzler, and X. Xie, Phys. Rev. A **94**, 033401 (2016).
[30] W. A. Chupka and J. Berkowitz, J. Chem. Phys. **51**, 4244 (1969).
[31] S. Takezawa, J. Chem. Phys. **52**, 2575 (1970).
[32] M. Beyer and F. Merkt, Phys. Rev. Lett. **116**, 093001 (2016).
[33] R. S. Berry, J. Chem. Phys. **45**, 1228 (1966).
[34] C. Jungen and S. T. Pratt, J. Chem. Phys. **133**, 214303 (2010).
[35] X. Xie, S. Roither, D. Kartashov, E. Persson, D. G. Arbó, L. Zhang, S. Gräfe, M. S. Schöffler, J. Burgdörfer, A. Baltuška, and M. Kitzler, Phys. Rev. Lett. **108**, 193004 (2012).
[36] D. Ray, F. He, S. De, W. Cao, H. Mashiko, P. Ranitovic, K. P. Singh, I. Znakovskaya, U. Thumm, G. G. Paulus, M. F. Kling, I. V. Litvinyuk, and C. L. Cocke, Phys. Rev. Lett. **103**, 223201 (2009).
[37] X. Gong, P. He, Q. Song, Q. Ji, H. Pan, J. Ding, F. He, H. Zeng, and J. Wu, Phys. Rev. Lett. **113**, 203001 (2014).
[38] M. Richter, M. Kunitski, M. Schöffler, T. Jahnke, L. P. H. Schmidt, and R. Dörner, Phys. Rev. A **94**, 033416 (2016).